Journal of Zhejiang University SCIENCE A
ISSN 1673-565X (Print); ISSN 1862-1775 (Online)
www.zju.edu.cn/jzus; www.springerlink.com
E-mail: jzus@zju.edu.cn

Automatic segmentation of bladder in CT images*

Feng SHI†[1], Jie YANG[1], Yue-min ZHU[2]

([1]*Institute of Image Processing and Pattern Recognition, Shanghai Jiao Tong University, Shanghai 200240, China*)

([2]*CREATIS, INSA of Lyon, University of Lyon 1, Villeurbanne, France*)

†E-mail: shifeng.sjtu@gmail.com

Received Mar. 6, 2008; Revision accepted June 1, 2008; Crosschecked Dec. 26, 2008

Abstract: Segmentation of the bladder in computerized tomography (CT) images is an important step in radiation therapy planning of prostate cancer. We present a new segmentation scheme to automatically delineate the bladder contour in CT images with three major steps. First, we use the mean shift algorithm to obtain a clustered image containing the rough contour of the bladder, which is then extracted in the second step by applying a region-growing algorithm with the initial seed point selected from a line-by-line scanning process. The third step is to refine the bladder contour more accurately using the rolling-ball algorithm. These steps are then extended to segment the bladder volume in a slice-by-slice manner. The obtained results were compared to manual segmentation by radiation oncologists. The average values of sensitivity, specificity, positive predictive value, negative predictive value, and Hausdorff distance are 86.5%, 96.3%, 90.5%, 96.5%, and 2.8 pixels, respectively. The results show that the bladder can be accurately segmented.

Key words: Image segmentation, Computerized tomography (CT), Mean shift, Bladder, Rolling ball
doi:10.1631/jzus.A0820157 **Document code:** A **CLC number:** TP391.4

INTRODUCTION

Delineation of the organs at risk is an important step in radiation therapy planning of prostate cancer. The bladder is considered as one of the organs at risk that should be protected against a high dose of radiation during treatment of prostate cancer (Costa *et al*., 2007). Due to the large variations of bladder geometry between patients and the limited contrast between the bladder and nearby organs, this work has been done traditionally by the radiation oncologists manually using simple drawing tools, which is not only time consuming, but also prone to errors and not reproducible, especially for a large dataset. Therefore, an automatic approach for accurate and reliable segmentation of the bladder in computerized tomography (CT) images is of great importance in radiation therapy planning.

A number of studies of bladder segmentation have been published in recent years. Mazonakis *et al.* (2001) used region growing and manual tracing to segment the bladder in CT images. However, a major limitation of region growing is the leaking problem, which makes this method not robust to most of the clinical situations. Camapum *et al*.(2004) used a multi-region–growing technique followed by watershed transform to segment the bladder automatically, and a morphological filter was applied in the post-processing step to improve the final segmentation. Unfortunately, this method could not prevent the extracted bladder contour from leaking into nearby organs when they share ambiguous boundaries. Bueno *et al*.(2004) delineated the bladder contour by evolving an active contour constrained to a fuzzy intensity image based on a fuzzy C-means clustering algorithm. The fuzzy reasoning in addition to statistical information was also used for final contour convergence. This method requires a set of manually placed points served as initial control points, and the placed points have a considerable influence on the accuracy of the results. Xu *et al.*(2003) presented a method using radial searching for bladder contour

* Project (No. 60675023) supported by the National Natural Science Foundation of China

detection. This method also ignores the impact of the nearby organs, and hence is only feasible on a limited dataset. Lee and Chung (2004) suggested identifying the bladder in CT images using shape descriptors, fuzzy rules and a fuzzy-inference-based neural network. A major limitation of this method is that the bladder shape is assumed to be compact and similar to a square. Freedman and Zhang (2005) introduced a semi-automatic segmentation approach by incorporating shape priors into a graph-cut framework. Whereas, the bladder shape is characterized by high variations and dictated by the filling that can be unpredictable. Hence, applying this method to the vast number of clinical data is unfeasible. Both Costa *et al.*(2007) and Rousson *et al.*(2005) suggested jointly segmenting the bladder and prostate by evolving two surfaces, and applied the prostate shape to constrain the deformation process. Costa *et al.*(2007) used an explicit representation of the surface by mesh, while Rousson *et al.*(2005) adopted an implicit representation by level set. However, the prostate non-rigidly differs from patient to patient. It is hard to adequately model the anatomical differences between patients. Furthermore, since both prostate position and shape are taken into account during model creation, too much deformation of the organ is not welcome at this point. Recently, Haas *et al.*(2008) used a flood-fill technique to extract the bladder region from CT images. This approach, while simple, does not produce accurate results due to its neglect of the influence of the nearby organs.

Initially introduced by Fukunaga and Hostetler (1975), the mean shift algorithm is a non-parameter clustering approach for feature space analysis and has been applied in many computer vision systems (Georgescu *et al.*, 2003; Li *et al.*, 2007). Mean shift gained popularity after the formulation was revised by Cheng (1995). The mean shift algorithm has the properties of unsupervised clustering, thus making it a powerful tool for image segmentation (Comaniciu and Meer, 2002). However, the mean shift segmentation process just partitions the image domain into a number of regions according to the intensity and spatial information, and most of the clustered regions are not of interest in the medical images (Jimenez *et al.*, 2003; Mayer and Greenspan, 2006). Therefore, using only the mean shift algorithm to segment medical images usually does not work well.

In this paper, we propose a hybrid scheme of automatic bladder segmentation, which combines mean shift clustering, line-by-line scanning and a rolling-ball filter. By constraining the clustering domain into a confined region via an area mask obtained from the segmentation result of the preceding slice, the impact of the nearby organs can be reduced.

METHODS

The proposed segmentation process starts by a selected slice, where the bladder has a large area profile. Three main steps are then performed for the segmentation of this selected slice. In the first step, the mean shift algorithm is carried out to obtain a clustered intermediate result containing the rough contour of the bladder, which is extracted in the second step by applying a seeded region-growing algorithm with the initial seed point determined through a line-by-line scanning process. The final step consists in employing the rolling-ball algorithm to refine the bladder contour more accurately. This 2D algorithm is then extended to segment the bladder volume in a slice-by-slice manner, except that for the non-selected slices, the seed point of the region-growing algorithm is estimated as the mass center of the bladder region extracted in the preceding slice.

Mean shift clustering

Let data be a finite set of pixel points $S=\{\boldsymbol{x}_i|i=1, 2, \ldots, n\}$ in the d-dimensional Euclidean feature space and let $\boldsymbol{y}_i^j$ denote each point at the jth mean shift iteration, where $\boldsymbol{y}_i^0 = \boldsymbol{x}_i$. The mean shift algorithm is formulated as

$$\boldsymbol{y}_i^{j+1} = \boldsymbol{y}_i^j + m(\boldsymbol{y}_i^j), \tag{1}$$

where $m(\boldsymbol{y}_i^j)$ is the mean shift vector,

$$m(\boldsymbol{y}_i^j) = \frac{\sum_{k=1}^{n} w\left(\left\|(\boldsymbol{y}_k^j - \boldsymbol{y}_i^j)/h\right\|^2\right)\boldsymbol{y}_k^j}{\sum_{k=1}^{n} w\left(\left\|(\boldsymbol{y}_k^j - \boldsymbol{y}_i^j)/h\right\|^2\right)} - \boldsymbol{y}_i^j. \tag{2}$$

In Eq.(2), w indicates a weight function, and h is a window size parameter.

A CT image can be represented as a 2D array of Hounsfield values. In our work, the feature space is a joint location-intensity domain concatenating location and intensity vectors (Comaniciu and Meer, 2002). After projecting the CT image into the feature space, all the vectors in this feature space are subsequently clustered by the mean shift algorithm. Let $\boldsymbol{x}_i$ (i=1, 2, …, n) be the original CT image points, $\{\boldsymbol{z}_i|i=1, 2, \ldots, n\}$ the set of points of convergence, and L_i (i=1, 2, …, n) the labels for different regions. As described in (Comaniciu and Meer, 2002), the details of the clustering process are as follows:

Step 1: For each i=1, 2, …, n, perform the mean shift algorithm for $\boldsymbol{x}_i$ and store the convergence point in $\boldsymbol{z}_i$.

Step 1.1: Initialize j=0 and $\boldsymbol{y}_i^j = \boldsymbol{x}_i$.

Step 1.2: Compute $m(\boldsymbol{y}_i^j)$ according to Eq.(1) and let $j=j+1$ until convergence.

Step 1.3: Assign $\boldsymbol{z}_i = \boldsymbol{x}_i^{\mathrm{s}} + \boldsymbol{y}_{\mathrm{conv}}^{\mathrm{r}}$ to specify that the clustered point at the spatial location of $\boldsymbol{x}_i$ has the range components of the point of convergence $\boldsymbol{y}_{\mathrm{conv}}$, where superscripts "s" and "r" represent the spatial and range components of a feature space vector, respectively.

Step 2: Delineate the clusters $\{C_j\}_{j=1, 2, \ldots, m}$ in the feature space by grouping together all $\boldsymbol{z}_i$, which are closer than h_{s} in the spatial domain and h_{r} in the range domain, i.e., to concatenate the basins of attraction of the corresponding convergence points.

Step 3: For each i=1, 2, …, n, assign $L_i=\{j|\boldsymbol{z}_i\in C_j\}$.

Step 4: Merge the regions in the spatial space that are smaller than M pixels into their neighboring regions.

Automatic extraction of the bladder

The image having now been segmented into separated regions, the next step is to automatically identify which of these clusters represents the bladder. Allowing for different imaging parameters, the bladder is located using the difference of intensity only. First, we scan the entire image in a line-by-line manner, and for each scanned line as shown in Fig.1c (see P244), the profile of the line is stored in an array $P=\{p_i|i=1, 2, \ldots, w\}$, where w (pixels) is the width of the image. The red line indicates the scanned line and the blue curve represents its profile. Next, the difference of the profile array $D=\{d_i|i=1, 2, \ldots, w-1\}$ is computed as $d_i=\|\boldsymbol{x}_{i+1}-\boldsymbol{x}_i\|$, and D is then thresholded according to

$$d_i = \begin{cases} 0, & d_i \le T_{\mathrm{d}}, \\ 1, & d_i > T_{\mathrm{d}}, \end{cases} \tag{3}$$

where T_{d} is set to 12 pixels in the present work. Then we find the longest fragment of array D containing 0. If the length of the fragment is greater than a preset threshold and this fragment lies in the middle of the image, this line is considered as lying in the bladder region. The threshold is set to 45 pixels experimentally. The center point of the fragment of the line is then chosen as the seed point, followed by performing the region-growing algorithm on the clustered image with this seed point. The region grows up to the bladder boundary. Hence the rough contour of the bladder is extracted.

Refinement of the bladder contour

Since the bladder contour obtained from mean shift clustering tends to deviate from the actual contour in some low-contrast areas, some regions outside the bladder, such as seminal vesicles, can be added and are false positives. The following step consists in refining the contour to remove the false positives using the rolling-ball algorithm along the bladder boundary (Armato *et al*., 1999). First, a 2D ball filter is constructed with radius-r pixels. The ball is placed tangential to the contour on an initial point, and then rolling along the contour until returning back to the starting point. Where the contour is properly convex, the ball will contact the contour at a single point. However, if an erroneous indentation is encountered, the ball will contact the contour at multiple points. The two endpoints of such indentation are then connected using linear interpolation to bridge the indentation.

Segmentation of the bladder volume

The 2D algorithm can be extended to segment the bladder volume in a slice-by-slice manner, where the result of the preceding slice constrains the segmentation of the adjacent slice.

In pelvic CT images, nearby organs of the bladder, such as the prostate and seminal vesicles, have similar intensities to the bladder, making the bladder's boundary ambiguous. Therefore, the

extracted bladder contour may leak into these nearby organs due to their similar intensities. In order to tackle this problem, the extracted bladder contour in the preceding slice is used to form an area mask, which will then be dilated by using a morphological operator. The dilated mask is applied to suppress the adjacent tissues of the bladder in the next slice. Fig.2 (see P244) illustrates the slice-by-slice procedure. In Fig.2a, the seminal vesicles are near the bladder and have intensities similar to those of the bladder. However, after being constrained by the mask (Fig.2c), most of the seminal vesicle tissues are eliminated. Hence, in most cases, the seminal vesicles have less impact on the segmentation result.

This slice-by-slice process is repeated until reaching the top and bottom ends of the bladder. At each end slice, a mask obtained from the result of this slice will cover a number of heterogeneous regions in the next slice.

EXPERIMENTAL RESULTS AND DISCUSSION

The proposed segmentation scheme was applied to 15 evaluation datasets containing 214 images. Besides, 7 training datasets of 98 images were selected to determine the optimal values of parameters. The dimensions of all slices are 512×512 pixels. The in-plane pixel size ranges from 0.68 mm to 0.93 mm; the slice thickness ranges from 3.0 mm to 5.0 mm.

Evaluation of the method

In order to assess the performance of the segmentation, the results were compared against those obtained by manual segmentation. Two radiation oncologists were invited to delineate the bladder contours of the datasets, and the mean contours were used as ground truth. Fig.1g corresponds to the manually delineated contour of the bladder in Fig.1a.

To access the quality of our results, several quantitative measures including sensitivity, specificity, positive predictive value (PPV) and negative predictive value (NPV) were measured:

$$D_{\text{sen}} = N_{\text{tp}} / (N_{\text{tp}} + N_{\text{fn}}), \tag{4}$$

$$D_{\text{spe}} = N_{\text{tn}} / (N_{\text{tn}} + N_{\text{fp}}), \tag{5}$$

$$D_{\text{PPV}} = N_{\text{tp}} / (N_{\text{tp}} + N_{\text{fp}}), \tag{6}$$

$$D_{\text{NPV}} = N_{\text{tn}} / (N_{\text{tn}} + N_{\text{fn}}), \tag{7}$$

where D_{sen}, D_{spe}, D_{PPV} and D_{NPV} represent the sensitivity, specificity, positive predictive value and negative predictive value, respectively; N_{tp}, true positive, is the number of bladder pixels labeled as the bladder; N_{fp}, false positive, is the number of non-bladder pixels falsely classified as the bladder; N_{tn}, true negative, is the number of non-bladder pixels labeled as the non-bladder; N_{fn}, false negative, is the number of bladder pixels falsely classified as the non-bladder.

Sensitivity is the fraction of bladder pixels correctly identified as belonging to the bladder. Specificity refers to the fraction of non-bladder pixels correctly identified as not belonging to the bladder. PPV is the fraction of pixels identified as the bladder by the scheme, which actually belongs to the bladder. NPV indicates the fraction of pixels identified as non-bladder by the scheme, which actually belongs to the non-bladder. Ideally, each experiment should have 100% specificity and 100% sensitivity.

Hausdorff distance (HD) (Huttenlocher *et al.*, 1993), which is defined as the maximum of the set of the shortest distances between corresponding points of the automatic results A and manual results M, was also used to describe the largest deviation between the manually and automatically segmented contours:

$$H(A,M) = \max(h(A,M), h(M,A)), \tag{8}$$

where

$$h(A,M) = \frac{1}{N_A} \sum_{\boldsymbol{a} \in A} \min_{\boldsymbol{m} \in M} \| \boldsymbol{a} - \boldsymbol{m} \|. \tag{9}$$

$H(A, M)$ is the Hausdorff distance, and N_A is the set of the shortest distances between corresponding points of the automatic results A.

Parameter settings

The algorithm uses several sets of parameters. In the mean shift step, the range parameter h_{r} and the smallest significant feature size M control the number of the clustered regions. A smaller h_{r} could yield more clusters, so it may break the bladder into several regions. While a larger h_{r} could produce fewer clusters and requires more computation time, some bladder details may also be eliminated. Our experiments on the 7 training datasets showed that the optimal values for these two parameters are 9.5 and 50, respectively, at which point computational efficiency was maximized without sacrificing clustering accuracy. The spatial parameter was set to 7 in the present work.

Concerning the contour refinement process, the radius r of the rolling ball influences the smoothness of the contour, and it is set according to the degree of the indentations presented on the rough contour of the bladder. If r is set too large, the refinement process could yield a smoother bladder contour by eliminating more bladder details; as such, the false negative error will be large. A smaller r may preserve more bladder details, but some adjacent soft tissues could leak into the bladder region in the results of the refinement process, which will increase the false positive error. The changes of the average values in specificity and sensitivity for 7 training datasets by varying the parameter r are illustrated in Fig.3, which shows a tradeoff between sensitivity and specificity. So we use the value of the cross point of the sensitivity and specificity curves to balance this trend. The optimal value of r was thus determined to be 5 pixels.

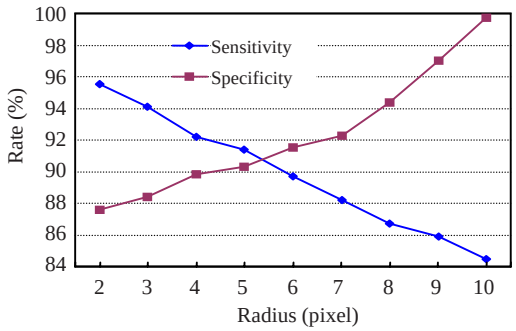

Fig.3 Changes of sensitivity and specificity by varying the radius of the rolling ball

Experiments on clinical data

Based on these parameters, our scheme was applied to 15 evaluation datasets. Fig.1 illustrates the images at intermediate steps in the process of our proposed method. Fig.1b shows the obtained clustering result of Fig.1a, in which the boundary of each cluster is highlighted by red color. Among these regions, only the region containing the bladder is of interest. The red boundary in Fig.1d is the rough contour of the bladder extracted by the region-growing algorithm, and Fig.1e shows the final segmentation result after the contour refining process. Fig.1f depicts the zoomed views of regions highlighted by blue circles in Fig.1d and Fig.1e, illustrating the effect of the rolling ball algorithm. Comparison of the results generated by our scheme and the contour given by the experts is shown in Fig.1h, in which the contour produced by our scheme (red) is superimposed on the manually delineated contour (blue). The comparison shows good agreement between the results generated by our method and manually by the experts.

We implemented our segmentation method on a Pentium IV PC with 2.6 GHz CPU and 2 GB RAM. The average processing time per slice was 3.7 s, and the delineation by experts took about 40 s per slice. Thus, our scheme was over 10 times faster than the manual segmentation.

To compare the results of our scheme with those of manual segmentation in each dataset, the sensitivity, specificity, PPV, NPV and HD were measured, as shown in Table 1. The average values of sensitivity, specificity, PPV, NPV and HD were 86.5%, 96.3%, 90.5%, 96.5%, and 2.8 pixels, respectively.

Table 1 Assessment of accuracy achieved by our scheme

Case No.	Sensitivity (%)	Specificity (%)	PPV (%)	NPV (%)	HD (pixel)
1	84.1	96.4	92.6	94.6	3
2	86.5	95.5	91.3	96.1	4
3	90.3	95.4	92.9	92.4	2
4	83.5	98.3	91.2	99.5	2
5	87.2	95.9	93.8	96.3	3
6	84.9	96.7	93.2	97.1	3
7	80.9	97.7	89.1	93.7	3
8	78.4	94.6	92.2	98.5	2
9	92.3	97.4	87.5	98.3	2
10	89.8	95.6	92.7	94.9	3
11	83.3	94.3	86.5	98.1	3
12	85.2	93.5	85.3	97.3	2
13	90.7	96.6	93.8	93.5	4
14	91.7	99.1	82.5	98.6	2
15	88.4	97.4	92.7	97.6	4
Average	86.5	96.3	90.5	96.5	2.8

PPV: positive predictive value; NPV: negative predictive value; HD: Hausdorff distance

Discussion

Errors in the computer results occurred mainly at the bladder-prostate interface. In the lower part the prostate appears next to the bladder. Due to the partial volume effect on some slices, even the radiologists have difficulty separating the prostate from the bladder. In such a situation, a large error could occur. There are 57 slices with the prostate next to the bladder, among which 13 slices contain such errors. However, we can reduce the effect of such errors by using the mask transferred from the preceding slice. Fig.4 illustrates such a case. Fig.4a is a slice where the bladder and the prostate have the same intensity

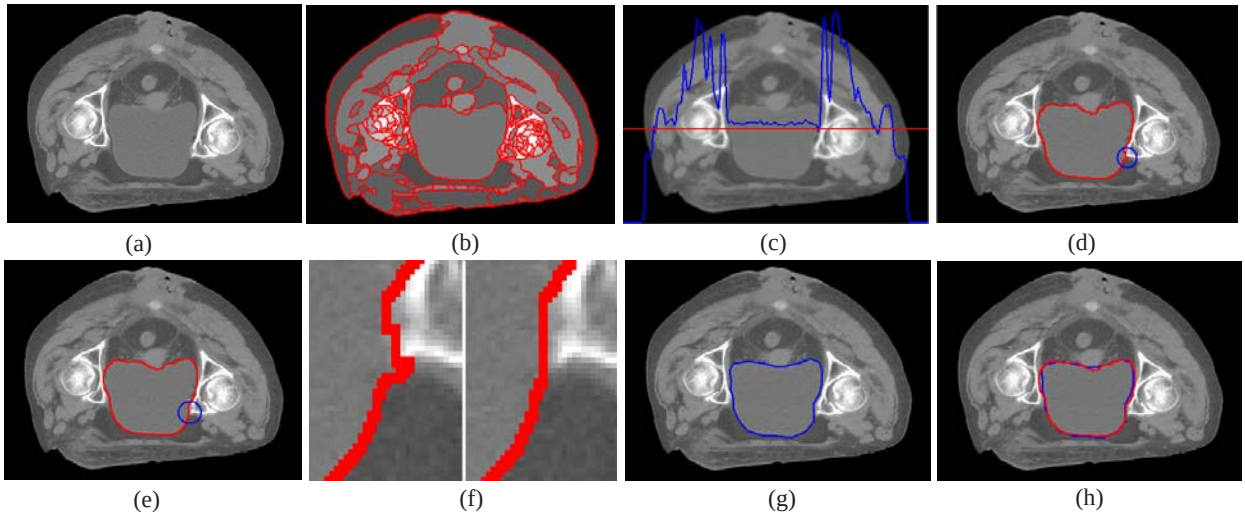

Fig.1 Intermediate results in the process of automatic segmentation. (a) Original image; (b) Clustered image by mean shift; (c) The profile (blue) of a scanning line (red); (d) Bladder contour extracted from the clustered image using a region-rowing algorithm; (e) Bladder contour refined by rolling ball algorithm; (f) Zoomed view of difference between pre-refinement (left) and post-refinement (right) of the bladder contour; (g) Mean contour manually delineated by two radiation oncologists; (h) Contour generated by our scheme (red) overlaps on the manually delineated contour (blue)

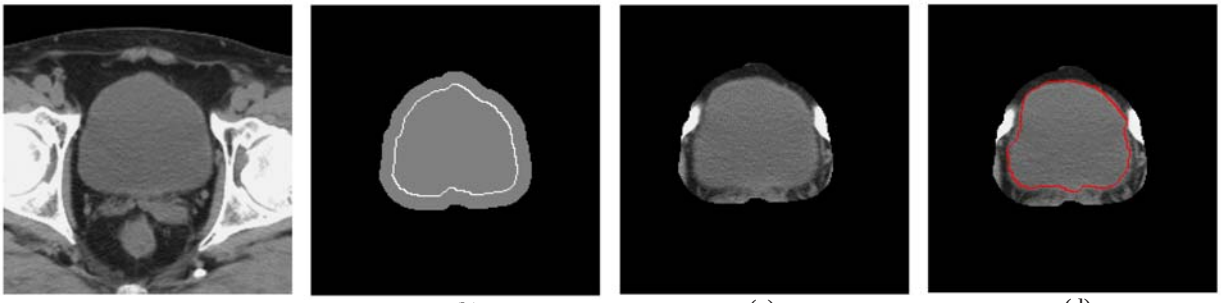

Fig.2 Segmentation of the bladder volume in a slice-by-slice manner. (a) A slice of the bladder volume; (b) The mask obtained from the previous adjacent slice of (a); (c) The confined area of (a); (d) Extracted bladder contour of (a)

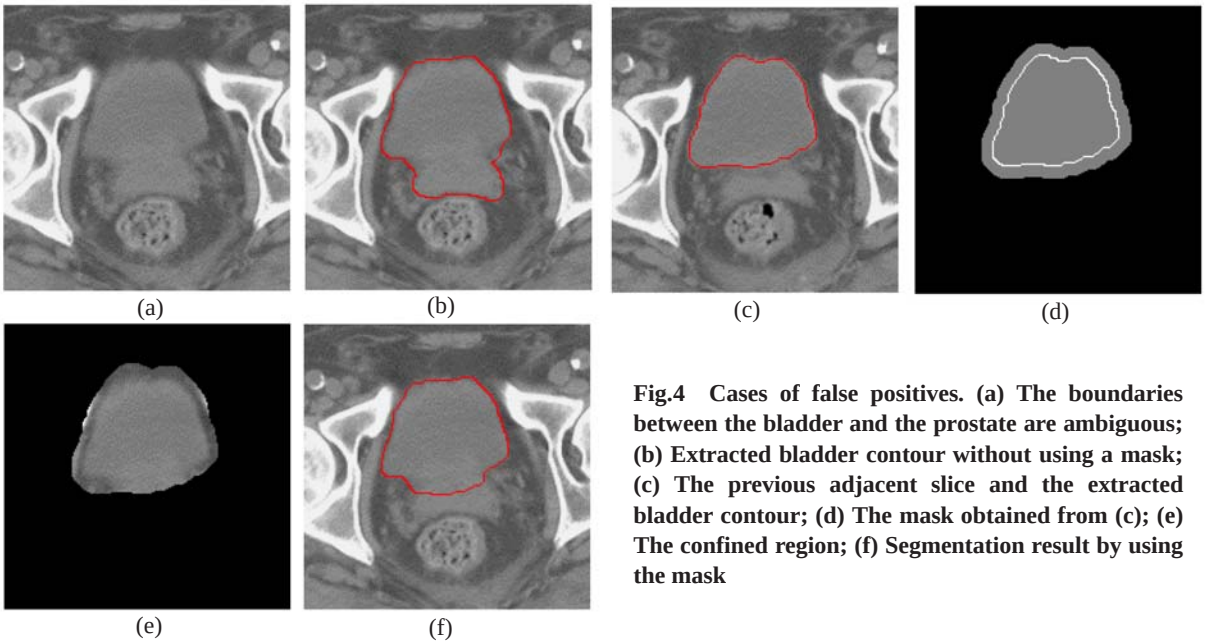

Fig.4 Cases of false positives. (a) The boundaries between the bladder and the prostate are ambiguous; (b) Extracted bladder contour without using a mask; (c) The previous adjacent slice and the extracted bladder contour; (d) The mask obtained from (c); (e) The confined region; (f) Segmentation result by using the mask

distribution, and there are no obvious boundaries between them. The delineated bladder contour without using a mask can be seen in Fig.4b, where the contour leaks into the prostate entirely due to the weak boundary. Fig.4c is the computer result of the preceding slice of Fig.4a, and Fig.4d is the mask computed from Fig.4c. Fig.4e is the confined region obtained by the mask. Fig.4f shows the extracted contour in the confined region, which prevents the contour from leaking too much into the prostate.

In order to better differentiate the bladder and the prostate, the knowledge of the experts should be incorporated into our framework in the form of a statistical model to delineate the contours of the bladder and the prostate simultaneously. This remains for the future work.

CONCLUSION

We have proposed an automatic bladder segmentation scheme for CT images. The method starts by a selected slice containing a large bladder profile; the mean shift algorithm is then performed to cluster the original CT image into a number of homogenous regions. In order to extract the bladder region from the clustered regions, the image is scanned line by line to obtain an initial point that is located in the bladder region. Taking this initial point as a seed point, we use a region-growing algorithm to extract the rough contour of the bladder. However, this rough contour tends to deviate from the actual contour in some low-contrast areas. The rolling-ball algorithm is then performed to refine the contour. This 2D algorithm is then extended to segment the bladder volume in a slice-by-slice manner.

We have validated the proposed scheme on 15 datasets of pelvic CT scans, and the results were compared with the mean of manual segmentation of two radiation oncologists. The average processing time is 3.7 s per slice, over 10 times faster than the manual segmentation. The average values of sensitivity, specificity, positive predictive value, negative predictive value, and Hausdorff distance are 86.5%, 96.3%, 90.5%, 96.5%, and 2.8 pixels, respectively. The results suggest that our method could be used for radiation therapy planning of prostate cancer, which requires an accurate segmentation of the bladder.

References

Armato, S.G.III, Giger, M.L., Moran, C.J., Blackburn, J.T., Doi, K., MacMahon H., 1999. Computerized detection of pulmonary nodules on CT scans. *RadioGraphics*, **19**:1303-1311.

Bueno, G., Martínez-Albalá, A., Adan, A., 2004. Fuzzy-snake Segmentation of Anatomical Structures Applied to CT Images. Int. Conf. on Image Analysis and Recognition, **2**:33-42.

Camapum, J.F., Silva, A.O., Freitas, A.N., Bassani, H.F., Freitas, F.M.O., 2004. Segmentation of Clinical Structures from Images of the Human Pelvic Area. Proc. 17th Brazilian Symp. on Computer Graphics and Image Processing, p.10-16. [doi:10.1109/SIBGRA.2004.1352937]

Cheng, Y., 1995. Mean shift, mode seeking, and clustering. *IEEE Trans. Pattern Anal. Mach. Intell.*, **17**(8):790-799. [doi:10.1109/34.400568]

Comaniciu, D., Meer, P., 2002. Mean shift: a robust approach toward feature space analysis. *IEEE Trans. Pattern Anal. Mach. Intell.*, **24**(5):603-619. [doi:10.1109/34.1000236]

Costa, M.J., Delingette, H., Novellas, S., Ayache, N., 2007. Automatic Segmentation of Bladder and Prostate Using Coupled 3D Deformable Models. 10th Int. Conf. on Medical Image Computing and Computer-assisted Intervention, p.252-260.

Freedman, D., Zhang, T., 2005. Interactive Graph Cut Based Segmentation with Shape Priors. IEEE Computer Society Conf. on Computer Vision and Pattern Recognition, **1**:755-762.

Fukunaga, K., Hostetler, L., 1975. The estimation of the gradient of a density function, with applications in pattern recognition. *IEEE Trans. Inf. Theory*, **21**(1):32-40. [doi:10.1109/TIT.1975.1055330]

Georgescu, B., Shimshoni, I., Meer, P., 2003. Mean Shift Based Clustering in High Dimensions: A Texture Classification Example. Proc. Ninth IEEE Int. Conf. on Computer Vision, **1**:456-463. [doi:10.1109/ICCV.2003.1238382]

Haas, B., Coradi, T., Scholz, M., Kunz, P., Huber, M., Oppitz, U., Andre, L., Lengkeek, V., Huyskens, D., van Esch, A., *et al*., 2008. Automatic segmentation of thoracic and pelvic CT images for radiotherapy planning using implicit anatomic knowledge and organ-specific segmentation strategies. *Phys. Med. Biol.*, **53**(6):1751-1771. [doi:10.1088/0031-9155/53/6/017]

Huttenlocher, D.P., Klanderman, G.A., Rucklidge, W.J., 1993. Comparing images using the Hausdorff distance. *IEEE Trans. Pattern Anal. Mach. Intell.*, **15**(9):850-863. [doi:10.1109/34.232073]

Jimenez, J.R., Medina, V., Yanez, O., 2003. Nonparametric MRI Segmentation Using Mean Shift and Edge Confidence Maps. Proc. SPIE, **5032**:1433-1441. [doi:10.1117/12.480121]

Lee, C.C., Chung, P.C., 2004. Identifying Abdominal Organs Using Robust Fuzzy Inference Model. IEEE Int. Conf. on Networking, Sensing and Control, **2**:1289-1294. [doi:10.1109/ICNSC.2004.1297133]

Li, J., Fang, X., Hou, J., 2007. Mean shift based log-Gabor wavelet image coding. *J. Zhejiang Univ. Sci. A*, **8**(4):620-624. [doi:10.1631/jzus.2007.A0620]

Mayer, A., Greenspan, H., 2006. Segmentation of Brain MRI by Adaptive Mean Shift. 3rd IEEE Int. Symp. on Biomedical Imaging: Nano to Macro, p.319-322. [doi:10.1109/ISBI.2006.1624917]

Mazonakis, M., Damilakis, J., Varveris, H., Prassopoulos, P., Gourtsoyiannis, N., 2001. Image segmentation in treatment planning for prostate cancer using the region growing technique. *Br. J. Radiol.*, **74**:243-248.

Rousson, M., Khamene, A., Diallo, M., Celi, J.C., Sauer, F., 2005. Constrained Surface Evolutions for Prostate and Bladder Segmentation in CT Images. First Int. Workshop on Computer Vision for Biomedical Image Applications, p.251-260. [doi:10.1007/11569541_26]

Xu, W., Amin, S.A., Haas, O.C.L., Burnham, K.J., Mills, J.A., 2003. Contour Detection by Using Radial Searching for CT Images. 4th Int. IEEE EMBS Special Topic Conf. on Information Technology Applications in Biomedicine, p.346-349. [doi:10.1109/ITAB.2003.1222550]